

Investigation of Delamination Induced by Trust force in Drilling of Glass/Epoxy Composites using Cohesive Zone Modeling and Acoustic Emission Methods

Milad Saeedifar^{*}, Mohamad Fotouhi^{*}, Mehdi Ahmadi Najafabadi^{*1}

** Non-destructive Testing Lab, Department of Mechanical Engineering, Amirkabir University of Technology, 424 Hafez Ave, 15914, Tehran, Iran*

Abstract

Glass fiber reinforced plastics (GFRP) are being increasingly utilized in engineering applications due to their high specific strength and stiffness. Drilling is a very common machining operation to assembly of laminated composite components. However, Delamination is a serious concern in the drilling of fiber reinforced composite materials, can reduce strength and stiffness of the structure. In this paper, push-down delamination induced by trust force in drilling of glass/epoxy composites, was investigated using Cohesive Zone Modeling (CZM) and Acoustic Emission (AE) methods. In order to simulation of delamination in simulated drilling process by CZM, first DCB, MMB and ENF specimens were loaded till the components of interlaminar fracture toughness (G_I and G_{II}) were determined. After that, simulation of actual specimen was done. Also, the behavior of delamination during the test was investigated using AE signals. The obtained results showed that the AE method and CZM technique could predicted initiation of delamination in composites under drilling process, accurately. Finally, it was concluded that the combination of AE and CZM techniques can be utilized for structural health monitoring of laminated composites.

Keywords: Delamination, Acoustic Emission, Cohesive Zone Modeling, Trust Force, Interlaminar Fracture Toughness

1. Introduction

Glass fiber reinforced plastics (GFRP) are being increasingly utilized in engineering applications due to their high specific strength and stiffness. Delamination in GFRP has been a subject of intensive research since many years. This failure mechanism can be caused by improper manufacturing, stresses between the layers of the composite, transversal load and impact. In many

¹. Corresponding author; Tel: (+98 21) 6454 3431; Fax: +98 21 8871 2838; Email address: ahmadin@aut.ac.ir

real conditions, delamination occurs mainly in mode I, mode II and the combination of these pure modes. Its effect on the structure may include a dramatic loss of residual strength and stiffness. [1]. Understanding the delamination initiation and propagation behavior is useful to produce structures with higher strength against crack growth [2].

Delamination is an insidious failure mode that is frequently present within the composite and it may easily escape detection [3]. Passive methods, such as AE, may improve the reliability and confidence of delamination detection [4-8]. AE technique uses a piezoelectric transducer to receive the first signs of damage in a structure. AE signal is a transient wave originated by the damage mechanisms such as matrix cracking, fiber failure, debonding of the matrix from fibers, etc. This technique is an appropriate tool to detect in-situ information about the damages that occur during initiation and propagation of delamination [8-10].

A huge amount of literature has been published on mode I delamination and investigation of this damage using AE monitoring [11-16]. Benmedakhene et al. [14] evaluate initiation and propagation of delamination in laminated composites under static and dynamic mode I loading using AE. They investigate damage mechanisms and AE behavior of the specimens under different loading rate. Refahi et al. [15, 16] study delamination in glass/polyester composites under mode I loading condition using AE. They determine the initiation of delamination and ranges of the parameters of AE signals of the damage mechanisms that occur during delamination. Arumugam et al. [17] investigate delamination and the damage mechanisms in glass/epoxy composite specimens under mode I loading using AE and Fast Fourier Transform (FFT) analysis. Taghizadeh et al. [18] classify the damage mechanisms during mode I delamination in polypropylene/epoxy composites using AE and Principal Component Analysis (PCA) methods.

On the other hand, little work has been done on the behavior of delamination in laminated composites using AE method when they are subjected to different loading conditions (i.e. mode II and mixed mode types). This is due to experimental difficulties related to unstable crack growth and crack tip closure during delamination propagation under these modes. These factors prevent a rigorous measurement of mode II and mixed mode interlaminar fracture toughness. Pashmforoush et al. [19] investigate damage mechanisms in glass/epoxy composite under three point bending loading using AE and k-means genetic algorithm. The results revealed that there are three clusters with separate frequency ranges, each one representing a distinct damage mechanism. The obtained

results showed good performance of the methods in the damage characterization of composite materials.

Yousefi et al. [20] evaluate delamination in laminated composites under mode II loading using AE and wavelet based signal processing.

The aim of this paper is to enhance some applicable and sensitive approaches, based on AE and fracture mechanics, to characterize delamination in glass/epoxy composites under mode I, II and mixed of these pure modes. In this paper, the behavior of delamination and the critical energy which is required for onset of this defect were studied using mechanical experimental data, FEM analysis (J-integral), AE method and the combination of mechanical and AE experimental data. The experimental data were obtained from the specimens when subjected to mode I, II and mixed mode I & II delamination tests. At first, the mechanical data were used to study the initiation and propagation behavior of delamination in the specimens with various lay-ups under different loading conditions. After that, critical interlaminar fracture energy of the specimens was evaluated using the introduced methods. It was found that the sentry function and FEM approaches provide the lower bound of the interlaminar fracture toughness values. There was a good agreement between these results and the results of NL method. However, the results obtained using the VIS and 5%/max methods represent the upper bound values.

2. Experimental Procedures

2.1 Materials and specimens preparation

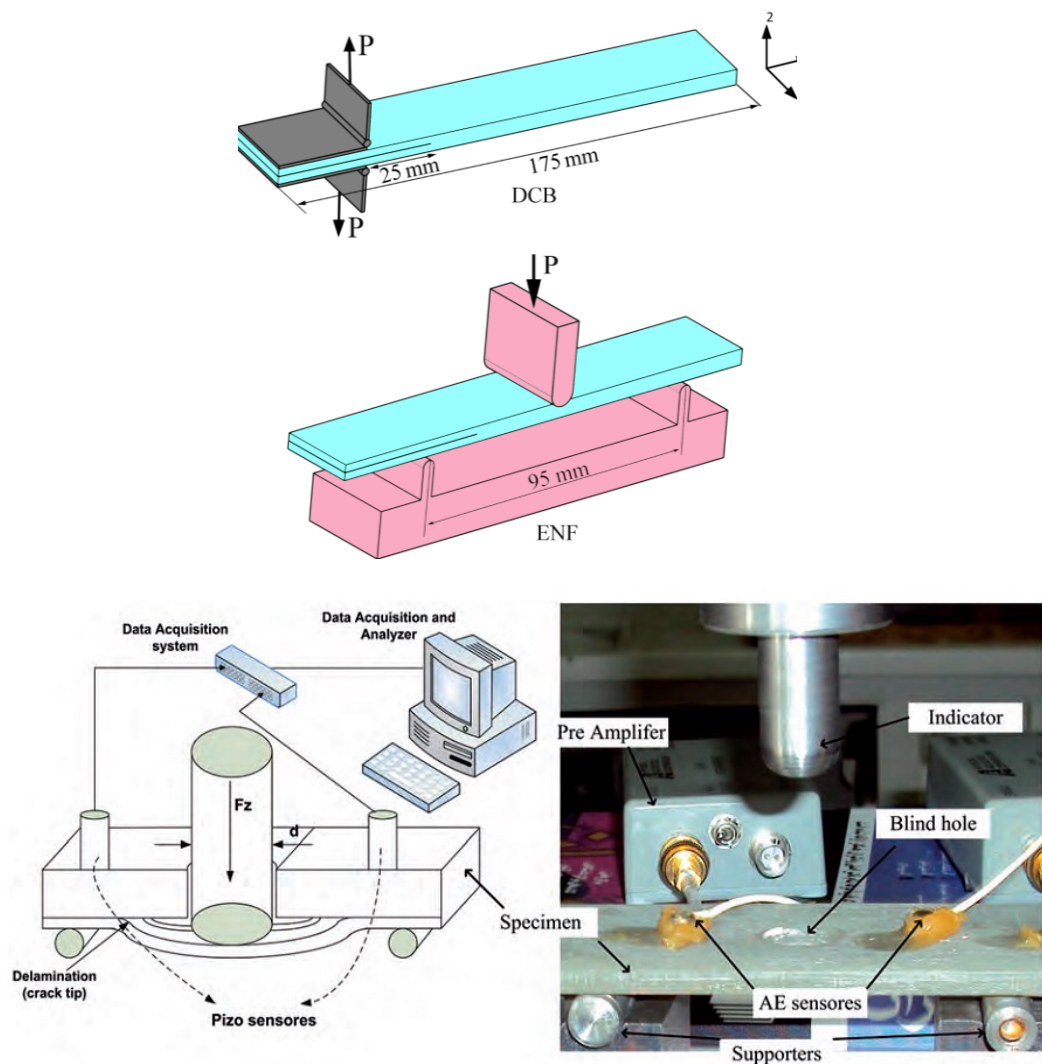
The experimental work was carried out on the epoxy resin reinforced by the E-glass unidirectional and woven fiber with the density of 1.46 g/cm³, 500 g/m² and 303 g/m², respectively. The laminates were provided by hand lay-up with compression molding. Two sets of specimens fabricated. First, DCB and ENF specimens with dimensions 180 mm×25 mm×5 mm fabricated. Then, Rectangular plates of cross glass fiber/epoxy composite plates with blind holes in the center were manufactured. The starter crack was created by inserting a Teflon film with a thickness of 20 μm during the molding process as an initial crack for the delamination test. The specimen dimensions were 150 mm×50 mm×5 mm. For ease of working, the woven specimen is named W and the unidirectional specimen is named U.

Table 1 Specification of the specimens

Fig. 1 Specimens geometry and dimensions

2.2 Test procedures

DCB and ENF test apparatus shown in Fig. 2 were used to apply the load to the laminated specimens. In DCB setup an upward force is applied to split end of the laminate to create Mode I. Whereas in ENF setup, a downward load is applied to the specimen center to create Mode II. The tests were carried out at a temperature of 24°C and at the constant displacement rate of 2 mm/min. The load and displacement were continuously measured and the crack length was visually recorded using a digital camera. The tests were iterated three times for each type of the specimen in a constant loading conditions. The actual specimens were placed in the testing machine and were subjected to the compression loads through three-point bending test.



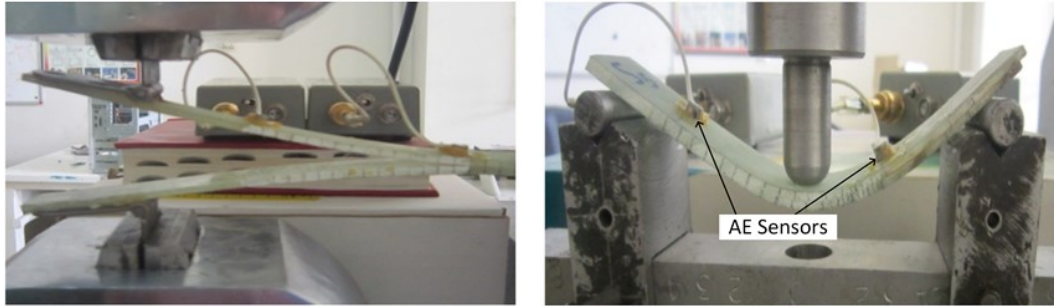


Fig. 2 Experimental setups for loading and the AE sensors; a) mode I, b) Mixed-mode I & II and c) Mode II

2.3 Testing machine

A properly calibrated tensile-compression test machine (HIWA) in the speed range from 0.5 to 500 mm/min was used in a displacement control mode with a constant crosshead speed. All the specimens were loaded with constant 2 mm/min crosshead rate.

2.4 AE device

AE events were recorded using AE software (AEWin) and a data acquisition system Physical Acoustics Corporation (PAC) PCI-2 with a maximum sampling rate of 40 MHz. PICO which is a broadband, resonant-type, single-crystal piezoelectric transducer from PAC, was used as the AE sensors. The sensors have a resonance frequency of 513.28 kHz and an optimum operating range of 100–750 kHz. In order to provide good acoustic coupling between the specimen and the sensors, surfaces of the sensors were covered with grease. The AE signals were detected by the sensors and enhanced by a 2/4/6-AST preamplifier. The gain selector of the preamplifier was set to 40 dB. The test sampling rate was 1 MHz with 16 bits of resolution between 10 and 100 dB. Prior to the damage check, the data acquisition system was calibrated for each kind of specimen, according to a pencil lead break procedure. The lead breakage operation was repeated several times and at different locations between the sensors. After the calibration step, AE signals were captured during mechanical testing using the sensors.

3. Fracture Toughness

3.1 Energy release rate

In a body with linear elastic behavior, strain energy release rate (G) is expressed by Eq 1:

$$G = -\frac{dU}{Bda} \quad (\text{Eq 1})$$

Where a, B and U are crack length, width and total elastic strain energy of the test specimens, respectively [21].

Energy release rate for mode I (DCB) and mode II (ENF) tests are as follows [22]:

$$G_I = \frac{12P^2a^2}{EB^2h^3} \quad (\text{Eq 2})$$

$$G_{II} = \frac{9P^2a^2}{16EB^2h^3} \quad (\text{Eq 3})$$

Where P is the applied load in different loading conditions. a, B, h and E are the delamination length, width of the specimens, half of the specimens thickness and elastic modulus, respectively. The dimensions, boundary conditions and loading conditions of the specimens are shown in Fig. 3.

Fig. 3 The dimensions, boundary conditions and loading conditions of the specimens configurations

3.2 Cohesive Zone Modeling

CZM is a technique in the framework of continuum damage mechanics that can predict initiation and propagation of delamination in the laminated composites [30]. CZM associates the tractions to the displacements at an interface where a crack may arise. The behavior of cohesive element is expressed by a traction–displacement curve. Previous research [33] illustrated that among the various constitutive curves employed for traction-displacement curve (such as exponential, trapezoidal, bi-linear, etc.) of the cohesive element, a bi-linear curve (See Fig. 3) has the best operation. The bi-linear curve has the following features [31]:

- a) An initial elastic region with the high stiffness (K) until the stress reaches to the interface strength (σ_{\max}).
- b) A following softening region until stress reaches to zero.

- c) The area beneath the curve is equal to the interlaminar fracture toughness (G_{IC}).

According to the above descriptions, when the stress of the cohesive element reaches to the interface strength, crack initiates and when the area beneath the bi-linear curve is equal to G_{IC} , the cohesive element failed and delamination propagates.

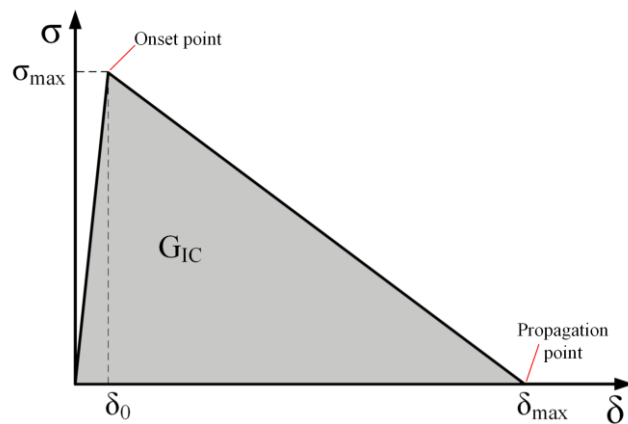


Fig. 3 Bi-linear constitutive equation of cohesive element

4. Results and discussion

4.1 Delamination behavior

The initiation and propagation of delamination and its potential interaction with other modes of failure are related to the crack tip conditions. Different loading conditions and lay-ups are the main reason for diversity of the crack tip conditions [24].

Normal stress in the crack tip is the cause of mode I delamination, when two layers are pulled apart, whereas shear stresses near the crack tip promote mode II (shear) propagation when sliding is observed [23].

Figures 5-7 show load-displacement and crack growth-displacement curves for the DCB, MMB and ENF specimens. Similar to Fig. 8, the load-displacement diagrams of the specimens can be divided into three regions: a) from the beginning to the nonlinearity point, b) from the nonlinearity point to the maximum load and c) from the maximum load to end of the test.

As can be seen from Figure 8, in region (a), by increasing load, the stored strain energy in the specimens is accumulated, but it does not reach to the critical value. Therefore, the delamination does not initiate. In region (b), the slope of the load-displacement diagram decreases. At the beginning of this region, the stored strain energy in the specimens reaches to the critical value and delamination initiates, but local strain hardening phenomenon arrests the crack growth [25]. In region (c), the delamination growth usually has unstable behavior. As is shown in Fig. 8 the applied load causes the large deflection of specimen W3, which results to the rupture of the specimen and there is a sudden drop of the load at displacement 25 mm.

Referring to the crack length diagrams, the comparison of Fig. 5-7 shows that the specimens U1 and W1 have steady state crack growth but crack growth behavior of the MMB and ENF specimens change during the tests. In the unidirectional specimens under different loading condition, due to fiber bridging during the delamination process, the load decreases slower than in the woven specimens and residual strength of these specimens are higher than in woven specimens.

Fig. 5 Load-displacement and crack length-displacement diagrams for specimens U1 and W1
(mode I)

Fig. 6 Load-displacement and crack length-displacement diagrams for specimens U2 and W2
(mixed-mode with $G_{II}/G_T = 30\%$)

Fig. 7 Load-displacement and crack length-displacement diagrams for specimens U3 and W3
(mode II)

Fig. 8 Three regions of the load-displacement diagram of specimen W3

4.2 Critical strain energy measurement

A delamination crack will initiate when the available energy release rate (G) is equal or greater than a critical value (G_C) [16]. This quantity is considered to be a material characteristic that represents the interlaminar fracture toughness of the laminated composites. As G reaches to critical value the crack initiates. Determination of G_C will help for better understanding of the damage tolerances and durability analyses of laminated composites.

G_C can be evaluated by different procedures. In this section, determination procedures are based on the mechanical information, FEM analysis, the AE information and the combination of mechanical and AE methods. Different procedures for evaluation of critical strain energy are presented in the following:

4.2.1 ASTM standards

For evaluation of G_C , critical load (P_C) must first be determined. For determination of P_C , the following procedures are presented in ASTM D5528 and ASTM D6671 standards [21, 22]:

- (a) Non linearity in the load–displacement diagram (NL),
- (b) Visual Inspection System (VIS) and
- (c) The compliance increase (5% max).

Figure 9 shows values of P_C which are obtained from the above methods for specimen W3.

Fig. 9 Critical load (P_C) values obtained from ASTM standard methods for specimen W3.

Table 2 shows values of fracture toughness of the specimens obtained from three methods introduced in the ASTM D5528 and ASTM D6771 standards.

Table 2 The G_C values obtained from ASTM standard methods for the specimens

4.2.2 Cohesive Zone Modeling

In this section, delamination growth is predicted using FEM simulation based on CZM technique. The material properties of the specimens are listed in Table 2.

Table 2 The material properties of the specimens.

Specimens	Parameters								
	E_1 (MPa)	E_2 (MPa)	E_3 (MPa)	ν_{12}	ν_{13}	ν_{23}	G_{12} (MPa)	G_{13} (MPa)	G_{23} (MPa)
U	28000	10600	7200	0.26	0.33	0.48	5600	3700	3200
W	17800	17800	7200	0.26	0.41	0.41	5600	3700	3700

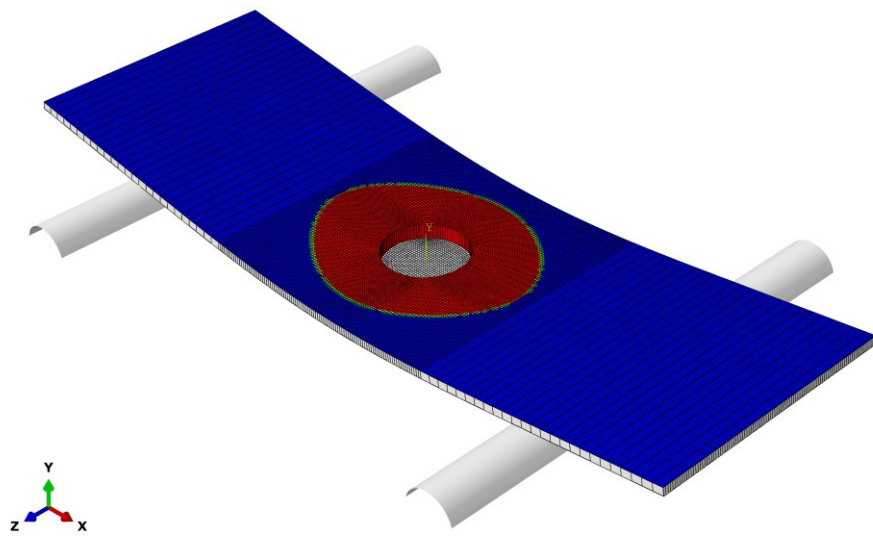
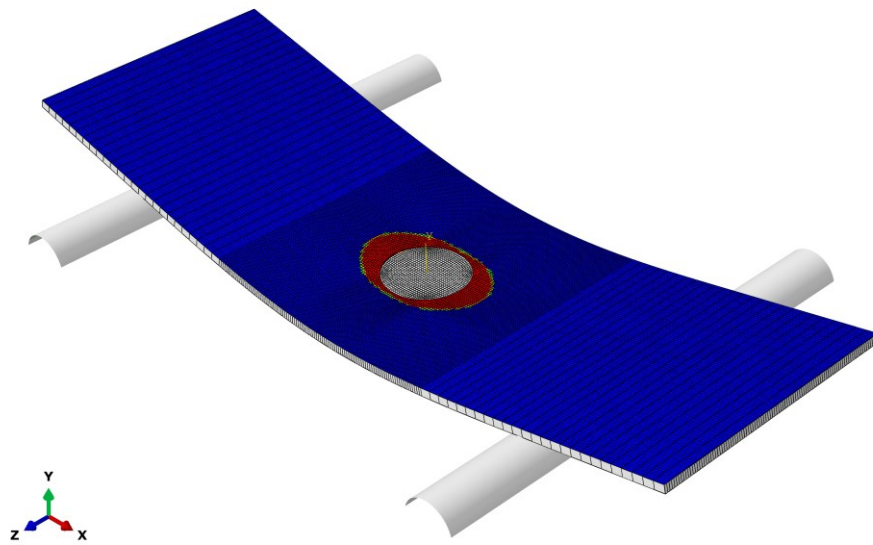
For composite section of the model, 2D, plane strain, continuum (solid) elements with 4 node and reduced integration formulation (CPE4R elements) are used. For the cohesive section, 2D cohesive elements with 4node (COH2D4) are used.

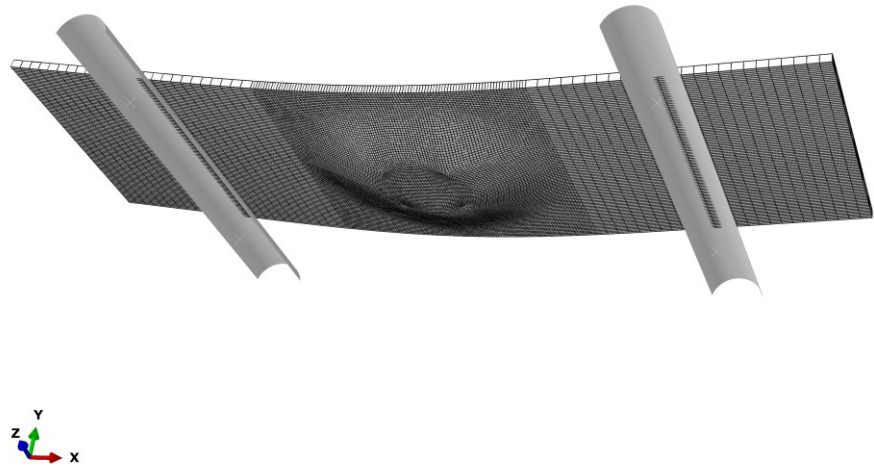
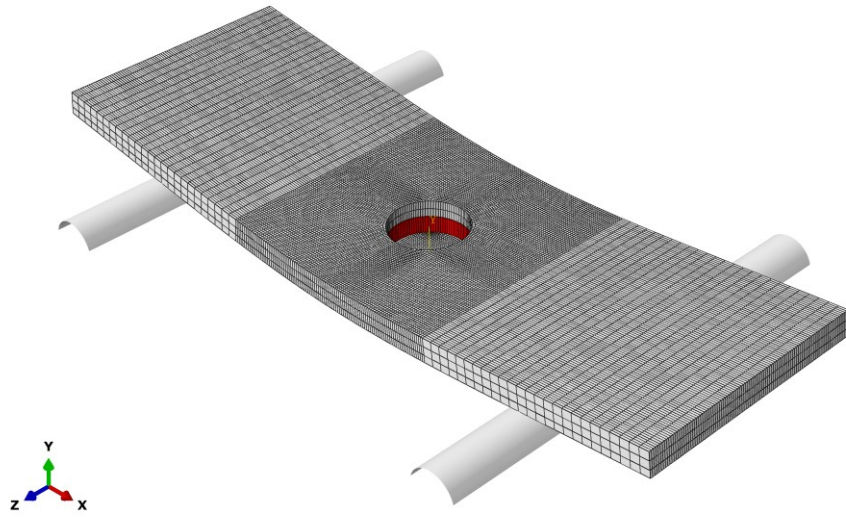
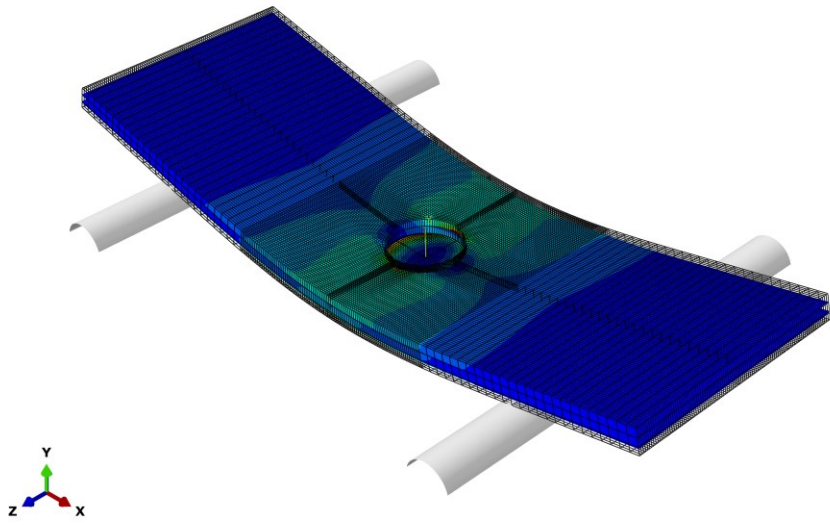
CZM results are very sensitive to the element size and in order to obtain accurate results very fine mesh must be utilized [29-31, 34-36]. Previous studies [29-31] indicated that for accurate simulation, at least two elements must be inserted in the cohesive zone length ahead the crack tip.

According to the obtained results, the parameters represented in Table 3 are used to simulate delamination in the DCB specimens. Figure 12 shows distribution of S_{33} stress in specimen U.

Table 3 The parameters of cohesive elements for simulation of delamination in the specimens.

Parameters				
Cohesive element length (mm)	σ_{\max} (MPa)	K(N/mm ³)	G_{IC} (kJ/m ²)	
			U_S	W_S
0.125	45	1e5	0.24	0.29





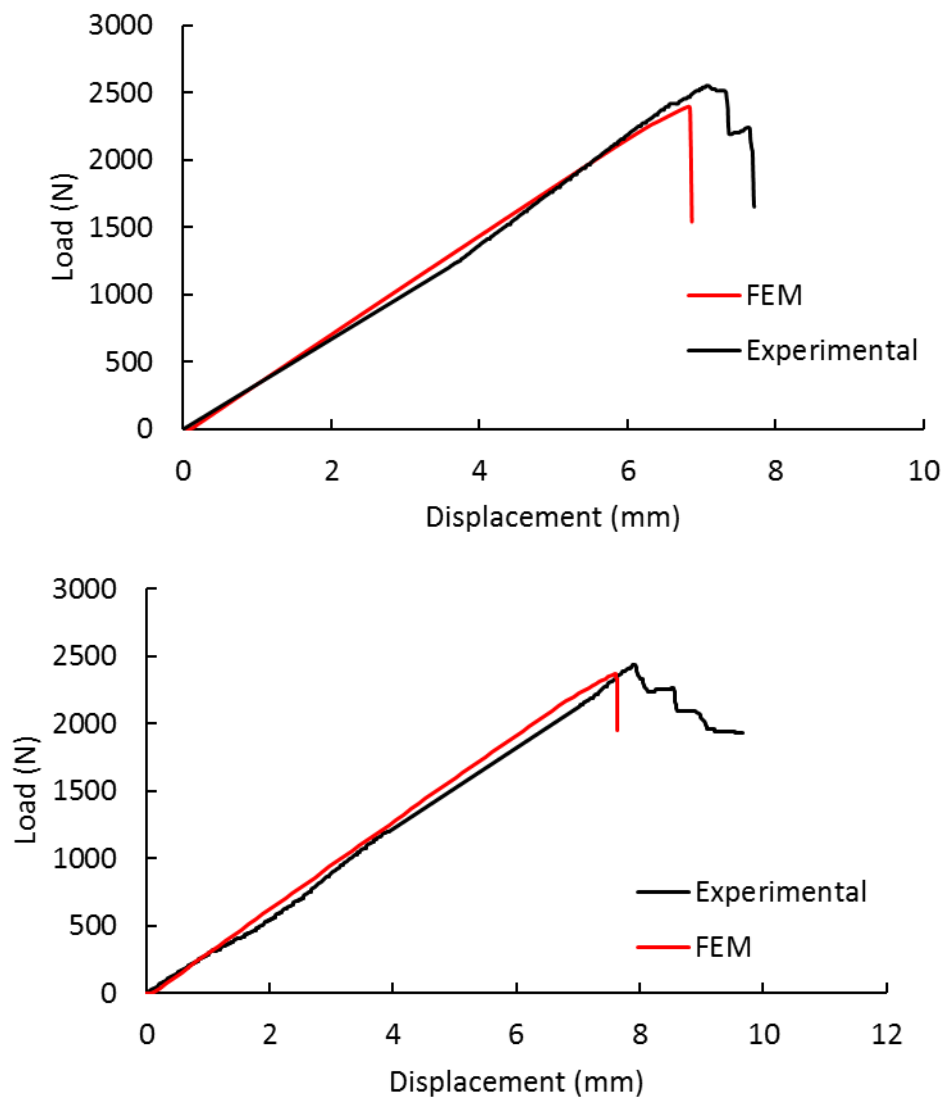


Fig. 12 Distribution of S_{33} stress in specimen U.

Figures 13 and 14 shows the load-displacement and crack growth- displacement curves obtained from simulation and Experimental results, for specimens U and W.

4.2.3 Acoustic Emission method

In analogy to the mechanical behavior of the specimens and existence of three regions in the load-displacement curves, similar trend in the acoustic emission behavior of the specimens is observed. These regions are illustrated for specimen U2 in Fig. 15. In region (a), no significant AE activity is observed. In region (b), by initiation of delamination the AE activities initiate and increase rapidly.

In region (c), by activation of damage mechanisms and growth of delamination in the specimens, AE activities with medium energy are observed.

Similar to the mechanical method, the critical load value can be determined using the AE information. In this section, for identification of critical load two methods are used: a) energy of AE signals and b) cumulative energy of AE signals which is sum of the energy of the recorded AE signals. In the first method, the load at the point at which first surge in the energy of AE signals is observed, is equal to P_C . Figure 16 shows the critical load (P_C) obtained by this method for specimen W1.

Sentry function

In the previous sections, mechanical information and AE information were used separately for characterization of the damage. Combination of mechanical data and AE information can also be used to have comprehensive damage characterization in the specimens. The function which is used for this combination is called sentry function. As indicated by Eq 6, the sentry function is stated in the logarithm form of the ratio of mechanical energy to acoustical energy [26]:

$$f(x) = Ln \left[\frac{E_s(x)}{E_a(x)} \right] \quad (\text{Eq 6})$$

Where $E_s(x)$, $E_a(x)$ and x are the strain energy (mechanical energy), the AE events energy and the displacement, respectively.

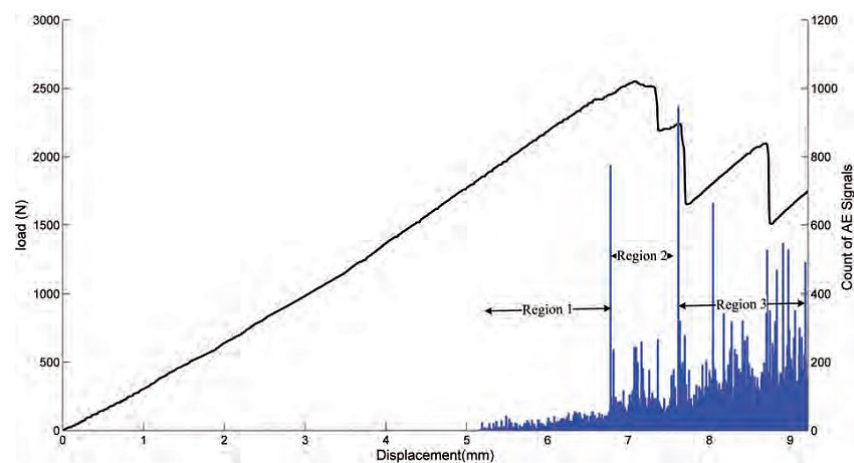


Fig. 15 The energy of AE signals, during the initiation and propagation of the delamination in specimen U2

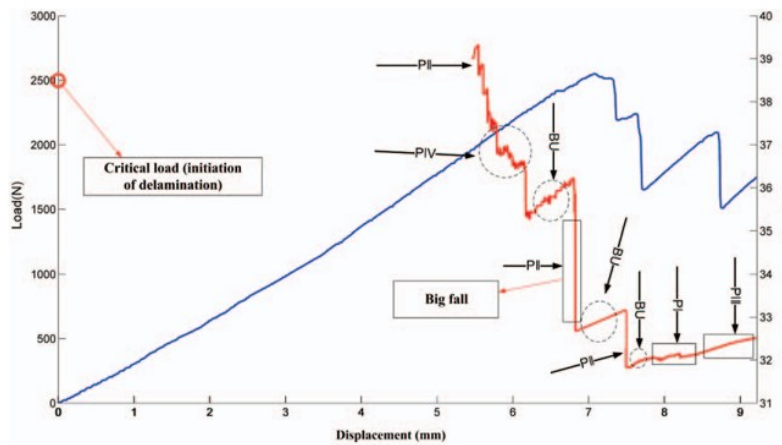
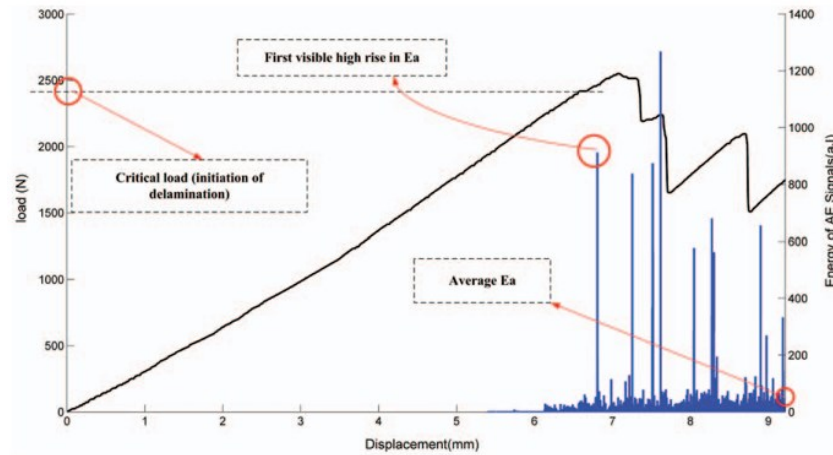


Fig. 16 Determination of critical load value using AE energy approach for specimen W1

In the second method, the load at the point at which first surge in the cumulative energy of AE signal appears is equal to P_C . Figure 17 shows the critical load (P_C) obtained by this method for specimen U1.

Fig. 17 Determination of critical load value using AE cumulative energy approach for specimen U1

Conclusion

This study focused on investigation of delamination in laminated composite materials and the following conclusions may be drawn:

- a) It was found that methods based on mechanical data and AE information are powerful procedures to characterize the initiation and propagation of the delamination in the glass/epoxy specimens under mode I (DCB), mode II (ENF) and mixed-mode I & II (MMB) loading conditions.

- b) The developed methods for evaluation of interlaminar fracture toughness for initiation of delamination, G_C , lead to the results which are in excellent agreement with the obtained results from ASTM standard methods and can solve their weaknesses, especially in mode II and mixed-mode conditions, where unstable crack growth and closed crack tip during delamination propagation preclude a rigorous measurement of G_C . In addition, these methods are easier and have higher repeatability compared with previous methods.
- c) The results obtained from FEM analysis and AE method, especially sentry function method, are shown to be more conservative than those derived from conventional fracture mechanics methodologies. This is due to the fact that AE monitoring is able to detect micro-damage mechanisms that occur before delamination is observed.
- d) It was also found that G_{II}/G_T modal ratio value and interface lay-up types cause different crack tip stress contributions and cause different damage mechanisms such as fiber breakage and matrix cracking during loading process. These fracture mechanisms are sources of the variation of mechanical information, AE parameters and interlaminar fracture toughness values. FEM results and SEM observation also used to evaluate appeared damage mechanisms. Finally it is concluded that AE examination is a powerful method for post-test and on-line analysis of delamination characteristics with less operator-dependent variations.

Acknowledgment

The authors wish to thank the Department of Mechanical Engineering at Amirkabir University of Technology, for providing the facilities for this study.

References

1. S. Sridharan, Delamination Behaviour of Composites, *CRC Press*, New York, 2008.
2. A.A. Bakhtiary Davijani, M. Hajikhani, M. Ahmadi, Acoustic Emission based on sentry function to monitor the initiation of delamination in composite materials, *Mater. Des.*, 2011, 32: 3059–3065.
3. A.B. de Moraes, A.B. Pereira, M.F.S.F. de Moura, A.G. Magalhães, Mode III interlaminar fracture of carbon/epoxy laminates using the edge crack torsion (ECT) test, *Compos. Sci. Technol.*, Volume 69, 2009, Issue 5, Pages 670–676.
4. I. Ndiaye, A. Maslouhi and J. Denault, Characterization of interfacial properties of composite materials by acoustic emission, *Polym. Compos.*, 2000, 21:595–604.

5. J. Bohse and A.J. Brunner, Acoustic emission in delamination investigation. In: S. Sridharan, Delamination behaviour of composites, *CRC Press*, New York, 2008, pp217–77.
6. G. Minak and A. Zucchelli, Damage evaluation and residual strength prediction of CFRP laminates by means of acoustic emission techniques, In: Durand LP, editor. Composite Materials Research Progress, *Nova Science Publishers Inc*, New York: 2008, pp. 165–207.
7. R. de Oliveira and A.T. Marques, Health monitoring of FRP using acoustic emission and artificial neural networks, *Comput. Struct.*, 2008, 86:367–73.
8. S. Huguet, N. Godin, R. Gaertner, L. Salmon and D. Villard, Use of acoustic emission to identify damage modes in glass fibre reinforced polyester, *Compos. Sci. Technol.*, 2002, 62(10–11):1433–44.
9. F. Pashmforoush, M. Fotouhi and M. Ahmadi, Acoustic emission-based damage classification of glass/polyester composites using harmony search k-means algorithm, *J. Reinf. Plast. Compos.*, 2012, 31: 671-680.
10. M. Fotouhi, H. Heidary, M. Ahmadi and F. Pashmforoush, Characterization of composite materials damage under quasi-static three-point bending test using wavelet and fuzzy C-means clustering, *J. Compos. Mater.*, 2012, 46(15):1795-1808.
11. I.A. Ashcroft, D.J. Hughes and S.J. Shaw, Mode I fracture of epoxy bonded composite joints: 1. Quasi-static loading, *Int. J. Adhes. Adhes.*, 2001; 21(2): 87–99.
12. A.B. de Morais, M.F. de Moura, A.T. Marques and P.T. de Castro, Mode-I interlaminar fracture of carbon/epoxy cross-ply composites, *Compos. Sci. Technol.*, 2002; 62(5): 679–686.
13. F. Perrin, M.N. Bureau, J. Denault, and J.I. Dickson, Mode I Interlaminar Crack Propagation in Continuous Glass Fiber/Polypropylene Composites: Temperature and Molding Condition Dependence, *Compos. Sci. Technol*, 2003, 63(5): 597-607.
14. S. Benmedakhene, M. Kenane, and M. L. Benzeggagh, Initiation and growth of delamination in glass/epoxy composites subjected to static and dynamic loading by acoustic emission monitoring, *Compos. Sci. Technol.*, 1999, vol.59, pp. 201-208.
15. M. Fotouhi and M. Ahmadi, Acoustic emission-based study to characterize the initiation of delamination in composite materials, *J. Thermoplast. Compos. Mater.*, DOI: 10.1177/0892705713519811, published online 21 January 2014.
16. A. Refahi Oskouei, A. Zucchelli, M. Ahmadi and G. Minak, An integrated approach based on acoustic emission and mechanical information to evaluate the delamination fracture toughness at mode I in composite laminate, *Mater. Des.*, 2011, 32(3):1444–1455.
17. V. Arumugam, S. Sajith, and A. Joseph Stanley, Acoustic Emission Characterization of Failure Modes in GFRP Laminates Under Mode I Delamination, *J. Nondestruct. Eval.*, 2011, Volume 30, Issue 3, pp 213-219.
18. J. Taghizadeh and M. Ahmadi, Identification of damage modes in polypropylene/epoxy composites by using principal component analysis on AE signals extracted from Mode I delamination, *Nondestruct. Test. Eva.*, 2012, Volume 27, Issue 2, pp. 151-170.
19. F. Pashmforoush, M. Fotouhi, and M. Ahmadi, Damage Characterization of Glass/Epoxy Composite under Three-Point Bending Test Using Acoustic Emission Technique, *J. Mater. Eng. Perform.*, 2012, 21:1380–1390.

20. J. Yousefi, M. Ahmadi, M. Nazmdar, A. Refahi, and F. Moghadas, Damage Categorization of Glass/Epoxy Composite Material under Mode II Delamination Using Acoustic Emission Data: A Clustering Approach to Elucidate Wavelet Transformation Analysis, *Arab. J. Sci. Eng.*, 2013, pp. 1-11.
21. ASTM D5528–01, Standard Test Method for Mode I Interlaminar Fracture Toughness of Unidirectional Fiber-Reinforced Polymer Matrix Composites, 2007.
22. ASTM D 6671/D 6671M – 03, Standard Test Method for Mixed Mode I-Mode II Interlaminar Fracture Toughness of Unidirectional Fiber Reinforced Polymer Matrix Composites, 2004.
23. T.L. Anderson, Fracture Mechanics; fundamentals and applications, *Taylor & Francis*, 2005, pp. 43 & 110.
24. I. Paris and A. Poursartip, Delamination Crack Tip Behavior at Failure in Composite Laminate under Mode I Loadings, *J. Thermoplast. Compos. Mater.*, 1998, 11: 57-69.
25. M.G. Andrews, R. Massabò, B.N. Cox, Elastic interaction of multiple delaminations in plates subject to cylindrical bending, *Int. J. Solids Struct.*, 2006, Volume 43, Issue 5, Pages 855–886.
26. G. Minak, P. Morelli and A. Zucchelli, Fatigue residual strength of circular laminate graphite–epoxy composite plates damaged by transverse load, *Compos. Sci. Technol.*, 2009, Volume 69, Issue 9, Pages 1358–1363.

List of Figure captions:

Fig. 1 Specimens geometry and dimensions

Fig. 2 Experimental setups for loading and the AE sensors; a) mode I, b) Mixed-mode I & II and c) Mode II

Fig. 3 The dimensions, boundary conditions and loading conditions of the specimens configurations

Fig. 4 An arbitrary path around the crack tip for evaluation the J-integral

Fig. 5 Load-displacement and crack length-displacement diagrams for specimens U1 and W1 (mode I)

Fig. 6 Load-displacement and crack length-displacement diagrams for specimens U2 and W2 (mixed-mode with $G_{II}/G_T = 30\%$)

Fig. 7 Load-displacement and crack length-displacement diagrams for specimens U3 and W3 (mode II)

Fig. 8 Three regions of the load-displacement curve of specimen W3

Fig. 9 Critical load (P_C) values obtained from ASTM standard methods for specimen W3

Fig. 10 Schematic of a) the discretized FE model and b) some of the contours

Fig. 11 Von Mises stress distribution in the specimens under: a) mode I, b) mixed-mode I & II and c) mode II loading conditions

Fig. 12 J-integral (is equal to G_C) values in 8 contours obtained from FEM analyses for the specimens U1 and W1 (mode I)

Fig. 13 Normal and shear stresses distribution in: a) mode I, b) mode II and c) mixed mode I & II loading condition

Fig. 14 SEM images of the damaged surfaces of the specimens under: a) mode I, b) mode II and c) mixed-mode I & II loading condition

Fig. 15 The energy of AE signals, during the initiation and propagation of the delamination in specimen U2

Fig. 16 Determination of critical load value using AE energy approach for specimen W1

Fig. 17 Determination of critical load value using AE cumulative energy approach for specimen U1

Fig. 18 The reference volumes in DCB specimen

Fig. 19 Determination of critical load value using sentry function approach for specimen W1

Fig. 20 The values of the G_C for the specimens which are obtained from the offered methods

List of Table captions:

Table 1 Specification of the specimens

Table 2 The G_C values obtained from ASTM standard methods for the specimens

Table 3 The material properties of the specimens

Table 4 The G_C values obtained from FEM analyses for the specimens

Table 5 The G_C values obtained from the AE energy, cumulative AE energy and sentry function methods for the specimens